Biological Problems, J. P. Tam and E. T. Kaiser, Eds. (Liss, New York, 1989), pp. 267–279; R. F. Nutt *et al.*, in *Peptides: Chemistry, Structure and Biology*, J. E. Rivier and G. R. Marshall, Eds. (ESCOM, Leiden, Netherlands, 1988), pp. 444–446.
9. W. J. Fairbrother, R. S. McDowell, B. C. Cunningham, *Biochemistry* **33**, 8897 (1994).
10. P. R. Bovy *et al.*, *J. Biol. Chem.* **264**, 20309 (1989).
11. T. W. von Geldern *et al.*, *J. Med. Chem.* **35**, 808 (1992).
12. S. H. Bass, R. Greene, J. A. Wells, *Proteins Struct. Funct. Genet.* **8**, 309 (1990); H. B. Lowman and J. A. Wells, *J. Mol. Biol.* **234**, 564 (1993); J. A. Wells and H. B. Lowman, *Curr. Opin. Struct. Biol.* **2**, 597 (1992).
13. Single-letter abbreviations for the amino acid residues are as follows: A, Ala; C, Cys; D, Asp; E, Glu; F, Phe; G, Gly; H, His; I, Ile; K, Lys; L, Leu; M, Met; N, Asn; P, Pro; Q, Gln; R, Arg; S, Ser; T, Thr; V, Val; W, Trp; and Y, Tyr. Mutations are designated by the wild-type residue, followed by its position and the mutant residue. Multiple mutations are indicated by a series of single mutations separated by hyphens.
14. B. Li and B. C. Cunningham, unpublished data.
15. The decrease (550 times lower) in bioactivity measured for the original 19-aa peptide compared with its 43 times lower receptor affinity may reflect a number of factors, including the susceptibility of this peptide to proteolysis in cell culture or kinetic parameters involved in receptor activation.
16. P. T. Jones, P .H. Dear, J. Foote, M. S. Neuberger, G. Winter, *Nature* **321**, 522 (1986); B. C. Cunningham, D. J. Henner, J. A. Wells, *Science* **247**, 1461 (1990); L. Presta, *Annu. Rep. Med. Chem.* **29**, 317 (1994).
17. J. A. Wells, W. J. Fairbrother, J. Otlewski, M. Laskowski, J. Burnier, *Proc. Natl. Acad. Sci. U.S.A.* **91**, 4110 (1994); D. R. Corey and M. A. Phillips, *ibid.*, p. 4106.
18. Peptides were synthesized on an Applied Biosystems 430A automated synthesizer according to standard *N-tert*-butoxycarbonyl chemistry protocols, cleaved off the resin with anhydrous HF at 0°C, then cyclized by the potassium ferricyanide method and purified by reversed-phase high-performance liquid chromatography. Masses of each peptide were verified by mass spectrometry. All the peptides except for variant 6 were synthesized with an amidated COOH-terminus.
19. Phagemid libraries that displayed variants of ANP contained codons that were randomized to all 20 amino acids by site-directed mutagenesis [T. A. Kunkel, J. D. Roberts, R. A. Zakour, *Methods Enzymol.* **154**, 367 (1987)] with the following oligonucleotides that changed target codons to NNS sequences (N is a mixture of all four bases and S is a mixture of G and C bases): 5′-TCTCTGGATAGATCTTGC(NNS)TTC(NNS)$_3$ ATGGATCGTATC(NNS)TGCCAGAGCGGT-3′ for library 1, 5′-ATGGATCGTATCGCGTGC(NNS)$_2$-GGGGGCGGCCC-3′ for library 2, 5′-ATGGATCGTATCGCGTGC-(NNS)$_3$-GGGGGCGGG-CCC-3′ for library 3, 5′-ATGGATCGTATCGCTGC(NNS)$_4$-GGGG-GCGGGCCC-3′ for library 4, and 5′-TATGCATCTCTGGATAGA-(NNS)TGC(NNS)TTCGGGGGCCGGATGGATCGTATC(NNS)TGC(NNS)CGGGGGGGCGGGTCT-3′ for library 5. Each library consisted of 4×10^7 to 22×10^7 independent mutants and theoretically represented all possible sequence combinations. To minimize wild-type background, the mutagenesis template used for libraries 2 to 5 was frameshifted within the region to be randomized.
20. The molecular models (Fig. 3) are from 1 of 11 energy-minimized structures of an ANP variant (*9*) whose coordinates are deposited in the Brookhaven Protein Data Bank (accession number 1ANP). This model of wild-type ANP contains two substitutions (L12M-S14R), which revert back mutations that were present in the variant whose structure was solved.
21. B. C. Cunningham, D. G. Lowe, B. Li, B. D. Bennett, J. A. Wells, *EMBO J.* **13**, 2508 (1994); B. D. Bennett *et al.*, *J. Biol. Chem.* **266**, 23060 (1991).
22. We thank D. Lowe for providing the immunoglobulin G–receptor fusion protein and for advice; B. McDowell for discussions; the DNA synthesis group for oligonucleotides; A. Padua for amino acid analysis; and D. Woods, K. Andow, and W. Anstine for help with graphics.

19 June 1995; accepted 18 October 1995

Sodium-Driven Potassium Uptake by the Plant Potassium Transporter HKT1 and Mutations Conferring Salt Tolerance

Francisco Rubio, Walter Gassmann, Julian I. Schroeder

Sodium (Na^+) at high millimolar concentrations in soils is toxic to most higher plants and severely reduces agricultural production worldwide. However, the molecular mechanisms for plant Na^+ uptake remain unknown. Here, the wheat root high-affinity potassium (K^+) uptake transporter HKT1 was shown to function as a high-affinity K^+-Na^+ cotransporter. High-affinity K^+ uptake was activated by micromolar Na^+ concentrations; moreover, high-affinity Na^+ uptake was activated by K^+ (half-activation constant, 2.8 μM K^+). However, at physiologically detrimental concentrations of Na^+, K^+ accumulation mediated by HKT1 was blocked and low-affinity Na^+ uptake occurred (Michaelis constant, ~16 mM Na^+), which correlated to Na^+ toxicity in plants. Point mutations in the sixth putative transmembrane domain of HKT1 that increase Na^+ tolerance were isolated with the use of yeast as a screening system. Na^+ uptake and Na^+ inhibition of K^+ accumulation indicate a possible role for HKT1 in physiological Na^+ toxicity in plants.

Salinization of irrigated lands is an increasing threat to agriculture. Na^+ concentrations [Na^+] of ≥25 mM are frequently found in saline soils, and most crop plants are glycophytes that are sensitive to high [Na^+] (*1*, *2*). Physiological studies indicate that Na^+ tolerance in plants is determined by several components (*1*, *2*), including osmolyte synthesis (*3*), Na^+ sensitivity of vital enzymes (*4*), and ion transport processes (*5*–*9*). It has been suggested that reducing Na^+ accumulation is crucial for engineering Na^+ tolerance in plants (*8*, *10*). However, the molecular mechanisms for Na^+ uptake and exclusion in plants remain unknown.

Recently, a complementary DNA (cDNA) from wheat, *HKT1*, was isolated that encodes a high-affinity K^+ uptake transporter (*11*), and in roots of *Arabidopsis thaliana*, voltage-clamp recordings of high-affinity K^+ uptake were reported (*12*). Current-voltage studies of the mechanism of K^+ uptake through HKT1 showed a variation in HKT1-mediated currents, which indicated that additional relevant transported factors remained unknown (*11*). Initial experiments showed that HKT1-mediated currents are affected by Na^+ (*11*). Here, we show that HKT1 mediates high-affinity K^+-Na^+ cotransport and low-affinity Na^+ uptake in a manner consistent with Na^+ toxicity in plants, and we identify mutations that improve HKT1-mediated Na^+ tolerance.

In control tracer flux experiments (*13*) with untransformed K^+ uptake–deficient yeast strains (*14*), neither $^{86}Rb^+$ (K^+) nor $^{22}Na^+$ uptake was observed (Fig. 1, filled symbols). In HKT1-expressing yeast cells, Na^+ strongly stimulated Rb^+ uptake (half-activation constant $K_{1/2}$ = 175 ± 50 μM Na^+, mean ± SD; n = 4) (Fig. 1A). $^{22}Na^+$ flux experiments in yeast allowed us to determine whether Na^+ uptake was mediated by HKT1 or whether Na^+ was merely enhancing Rb^+ accumulation (*15*). $^{22}Na^+$ uptake experiments in HKT1-expressing yeast demonstrat-

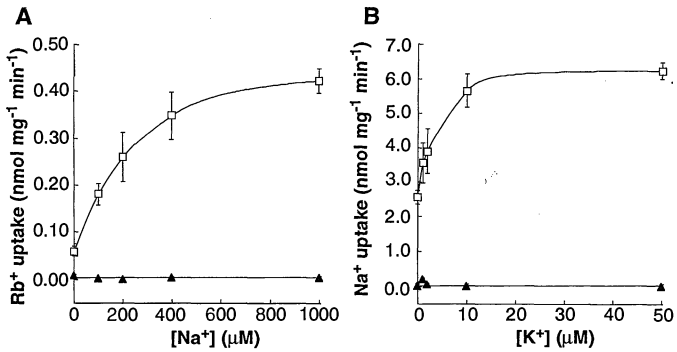

Fig. 1. HKT1 expressed in yeast gives rise to Na^+-stimulated Rb^+ uptake (**A**) and to K^+-stimulated Na^+ uptake (**B**) [□, yeast cells expressing HKT1; ▲, K^+ uptake–deficient yeast mutants (*14*)]. In (A), the initial rate of Rb^+ uptake is represented as a function of increasing external Na^+. In (B), the initial rate of Na^+ uptake is represented as a function of increasing external K^+. Uptake experiments were carried out at pH 6.0, 30°C, in the presence of 15 μM Rb^+ (A) or 200 μM Na^+ (B) (*13*). At nominally 0 [Na^+], a Rb^+ uptake rate of 0.05 nmol mg^{-1} min^{-1} was observed (A), and at nominally 0 [K^+], a Na^+ uptake rate of 2.6 nmol mg^{-1} min^{-1} was observed (B). This can likely be attributed to the background [Na^+] (11 μM) and [K^+] (2 μM) in the buffer used for the uptake experiments, as determined by atomic absorption spectrophotometry.

ed that Na^+ uptake was mediated by HKT1 (Fig. 1B). Moreover, K^+ stimulated the uptake of Na^+ ($K_{1/2}$ = 2.8 ± 0.3 μM K^+; n = 3) (Fig. 1B). HKT1-mediated Rb^+ uptake was not affected by external pH (*16*).

Cotransport of K^+ and Na^+ was directly quantified by studies of HKT1-mediated currents in *Xenopus* oocytes (*17*). Extracellular simultaneous perfusion with 1 mM Na^+ and 0.3 mM K^+ produced downward deflections in the current trace that were larger than those produced with 1 mM Na^+ or 0.3 mM K^+ alone (n = 21) (Fig. 2A). Absolute current values showed that Na^+ or K^+ alone merely reduced positive (outward) current (Fig. 2A) (*11*). However, the combined addition of Na^+ and K^+ produced inward currents and cation uptake (Fig. 2A). Additional experiments suggested that among the alkali metal cations (Li^+, Na^+, K^+, Rb^+, and Cs^+), Na^+ was at least 10 times as effective as any of the other cations in activating K^+ uptake (n = 5 for each cation) (*18*). Uninjected oocytes did not show currents under the same conditions (n = 33) (Fig. 2B).

In contrast to Na^+-free conditions (*11*), the simultaneous exposure of HKT1-expressing oocytes to Na^+ and K^+ produced stable reversal potentials (n = 55). Therefore, the identity of the ions transported by HKT1 in oocytes could be unequivocally established by determining absolute shifts in reversal potentials of HKT1-mediated steady-state currents under varying external [Na^+] or [K^+] (Fig. 2, C and D). HKT1-mediated steady-state currents in oocytes were insensitive to external pH in the range of pH 5 to 8 (n = 11) (*16*). Increasing external [Na^+] from 0.3 to 10 mM, with [K^+] constant at 1 mM, produced shifts of current-voltage curves toward more positive potentials (Fig. 2C), which confirmed that Na^+ was taken up by HKT1. At 1 mM external [Na^+], increasing [K^+] from 0.3 to 10 mM caused shifts in reversal potentials that were more pronounced (Fig. 2D). An increase in [K^+] from 1 to 10 mM caused a shift of +38 ± 6 mV (n = 8), whereas an increase in [Na^+] from 1 to 10 mM caused a shift of +22 ± 4 mV (n = 9). This result would be consistent with a transport stoichiometry of 1.7 K^+ to 1 Na^+ (*19*). Uptake experiments in yeast with micromolar concentrations of K^+ ($^{42}K^+$) and Na^+ ($^{22}Na^+$) showed a stoichiometry of 2.1 ± 0.5 to 1 (n = 8), which is in agreement with results obtained in oocyte experiments.

We next investigated the effect of phytotoxic high millimolar concentrations of Na^+ (>25 mM) on HKT1-mediated K^+ uptake in yeast. At a physiological [K^+] (100 μM), high [Na^+] inhibited the growth of HKT1-expressing yeast cells (Fig. 3A, left). This finding enabled us to design a strategy for isolating HKT1 mutants, using yeast as a screening system to identify domains in HKT1 responsible for Na^+ toxicity. HKT1 mutants were isolated (*20*) that allowed yeast cells to grow in the presence of 300 mM Na^+ and 0.1 mM K^+ (Fig. 3A, center and right). Two strongly Na^+-tolerant mutations were obtained, $Ala^{240} \rightarrow Val^{240}$ and $Leu^{247} \rightarrow Phe^{247}$, that were both located in the sixth hydrophobic domain of HKT1. The growth rates of yeast cells expressing the two mutated versions and the wild-type HKT1 showed no differences in the presence of nontoxic micromolar concentrations of Na^+. In addition, at low micromolar cation concentrations, the two mutants and the wild type showed similar rates of high-affinity Rb^+ and Na^+ uptake (n = 30) (*21*). However, at 300 mM Na^+ and 0.1 mM K^+, yeast cells expressing the A240V and L247F mutations (*22*) showed growth rates far in excess of that of the strain expressing wild-type HKT1 (Fig. 3B, inset).

Tracer flux experiments in yeast showed inhibition of HKT1-mediated Rb^+ uptake

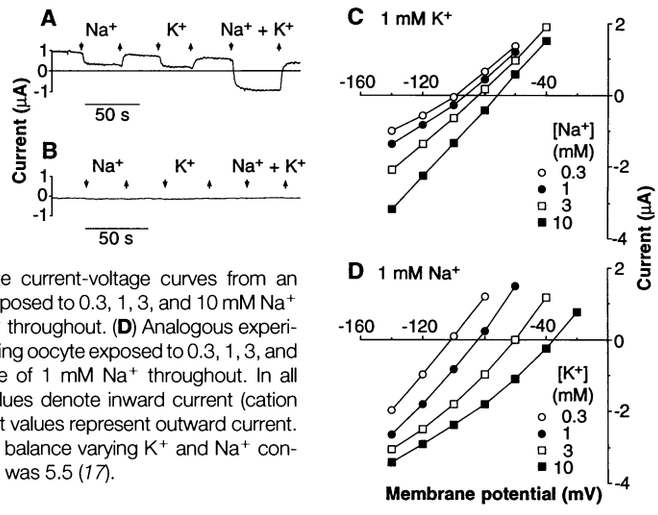

Fig. 2. HKT1 expressed in oocytes gives rise to Na^+-coupled K^+ uptake. (**A**) Exposure of an HKT1-expressing oocyte to 1 mM Na^+, 0.3 mM K^+, and 1 mM Na^+ plus 0.3 mM K^+. (**B**) Uninjected oocyte treated as in (A). The membrane potential in (A) and (B) was held at −120 mV. (**C**) Steady-state current-voltage curves from an HKT1-expressing oocyte exposed to 0.3, 1, 3, and 10 mM Na^+ in the presence of 1 mM K^+ throughout. (**D**) Analogous experiment with an HKT1-expressing oocyte exposed to 0.3, 1, 3, and 10 mM K^+ in the presence of 1 mM Na^+ throughout. In all panels, negative current values denote inward current (cation uptake), and positive current values represent outward current. Tris-glutamate was used to balance varying K^+ and Na^+ concentrations; the external pH was 5.5 (*17*).

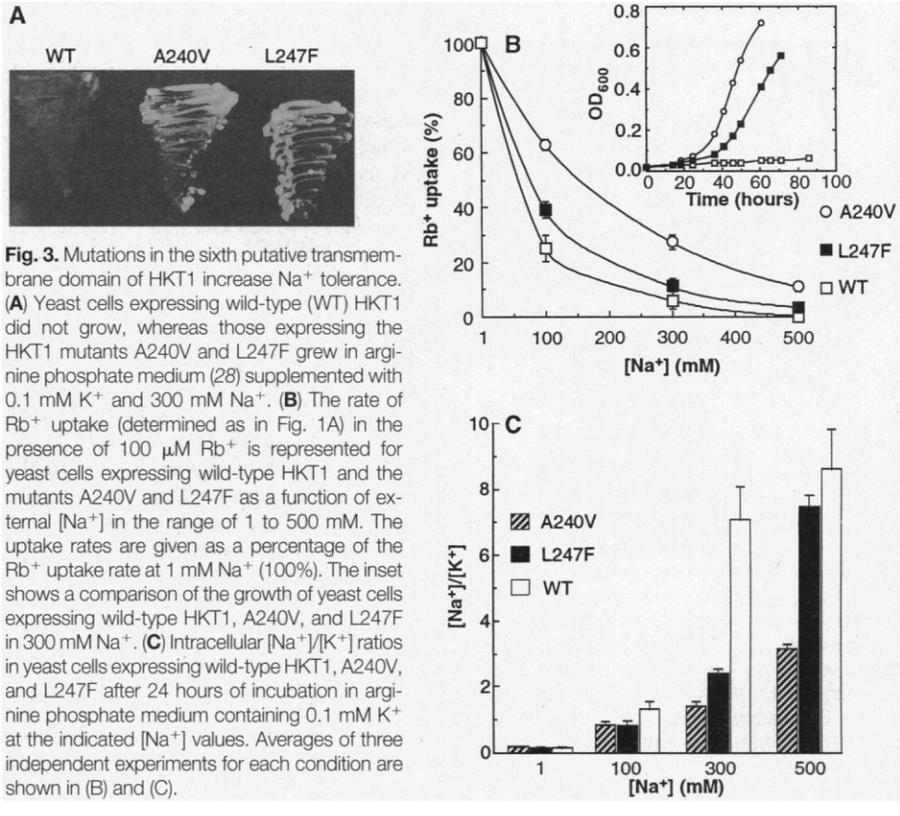

Fig. 3. Mutations in the sixth putative transmembrane domain of HKT1 increase Na^+ tolerance. (**A**) Yeast cells expressing wild-type (WT) HKT1 did not grow, whereas those expressing the HKT1 mutants A240V and L247F grew in arginine phosphate medium (*28*) supplemented with 0.1 mM K^+ and 300 mM Na^+. (**B**) The rate of Rb^+ uptake (determined as in Fig. 1A) in the presence of 100 μM Rb^+ is represented for yeast cells expressing wild-type HKT1 and the mutants A240V and L247F as a function of external [Na^+] in the range of 1 to 500 mM. The uptake rates are given as a percentage of the Rb^+ uptake rate at 1 mM Na^+ (100%). The inset shows a comparison of the growth of yeast cells expressing wild-type HKT1, A240V, and L247F in 300 mM Na^+. (**C**) Intracellular [Na^+]/[K^+] ratios in yeast cells expressing wild-type HKT1, A240V, and L247F after 24 hours of incubation in arginine phosphate medium containing 0.1 mM K^+ at the indicated [Na^+] values. Averages of three independent experiments for each condition are shown in (B) and (C).

Department of Biology and Center for Molecular Genetics, University of California, San Diego, La Jolla, CA 92093–0116, USA.

with increasing $[Na^+]$ in the range of 1 to 500 mM (Fig. 3B, lower trace). Millimolar concentrations of Na^+ inhibit K^+ uptake in plants (*6*, *12*), which could lead to K^+ deficiency. In the Na^+-tolerant HKT1 mutants, the rate of high-affinity Rb^+ uptake was less reduced by high $[Na^+]$ than in the wild type (n = 9) (Fig. 3B). The more Na^+-resistant mutant, A240V, showed less inhibition of Rb^+ uptake (Fig. 3B). The Na^+ concentrations at which Rb^+ uptake was reduced to 50% were 58 ± 5.3 mM Na^+ (wild-type HKT1), 154 ± 6.1 mM Na^+ (A240V), and 77 ± 5 mM Na^+ (L247F) (n = 3).

To determine whether additional differences in Na^+ accumulation occurred in the HKT1 mutants, we used atomic absorption spectrophotometry to quantify the internal Na^+ and K^+ contents in yeast cells growing in the presence of Na^+. At $[Na^+] > 100$ mM, the intracellular $[Na^+]/[K^+]$ ratio was the highest for the wild-type HKT1 and the lowest for the more Na^+-resistant mutant, A240V (Fig. 3C). The concentration sums of the two cations did not show any significant differences between the wild-type HKT1 and the mutants (*23*). These data show that at high $[Na^+]$, the Na^+-tolerant mutants allowed improved HKT1-mediated Rb^+ (K^+) accumulation and simultaneously reduced Na^+ uptake.

At high millimolar concentrations of Na^+, Na^+ ions may occupy the high-affinity K^+ binding site, thereby inhibiting K^+ uptake (Fig. 3B) and allowing increased Na^+ uptake (Fig. 3C) (*23*). To test this hypothesis, we studied currents in oocytes at high millimolar concentrations of Na^+ or K^+. In uninjected control oocytes, $[Na^+]$ or $[K^+]$ in the range of 1 to 100 mM did not produce inward currents (n = 14) (Fig. 4). In HKT1-expressing oocytes, external $[K^+]$ in the range of 1 to 100 mM in the absence of Na^+ reduced outward currents (*11*), but could not stimulate appreciable inward currents; this result underscores the necessity of Na^+ coupling for K^+ uptake (n = 9) (Fig. 4A). Similarly, 100 mM Li^+, Rb^+, or Cs^+ produced inward currents within the resolution range (n = 8) (*24*, *25*). However, for 10 to 100 mM Na^+ in the absence of external K^+, Na^+ was able to generate large inward (negative) currents (n = 9) (Fig. 4B). From the HKT1-mediated inward Na^+ conductances between –120 and –140 mV (Fig. 4B), an apparent Michaelis constant K_m of 16 ± 3 mM Na^+ (n = 5) was determined for low-affinity HKT1-mediated Na^+ uptake. In the A240V and L247F mutants, inward Na^+ currents at 100 mM Na^+ and 0 K^+ were reduced to 33% ± 10% (A240V, n = 17) and 66% ± 22% (L247F, n = 11) of the wild-type value. These data lend support to the hypothesis that toxic Na^+ concentrations block HKT1-mediated K^+ uptake by competing for high-affinity K^+ binding.

We conclude that HKT1 acts as a Na^+-coupled cotransporter, even though Na^+-coupled transport has been classically thought not to occur in higher plants (for reviews, see *1*, *9*, *26*). Na^+-coupled K^+ transport has been reported in charophyte algae (*27*). Coupling of K^+ uptake to the Na^+ gradient can be estimated to provide plant cells with sufficient K^+ for plant nutrition from soil solution K^+ concentrations of ~1 μM (*19*).

Previous studies have suggested that Na^+ toxicity is accompanied by low-affinity Na^+ uptake and by inhibition of high-affinity K^+ uptake (*5*, *6*, *12*). Our results indicate that HKT1 mediates low-affinity Na^+ uptake (Fig. 4B), and that at physiologically toxic $[Na^+]$ high-affinity K^+ uptake through HKT1 is inhibited (Fig. 3, B and C). HKT1 mutants were isolated that conferred increased Na^+ tolerance to yeast (Fig. 3A) and that showed less inhibition of K^+ uptake by high $[Na^+]$ as well as reduced Na^+ uptake (Fig. 3, B and C) (*23*). Because the mutations were located in the sixth putative transmembrane domain, this domain may be involved in low-affinity Na^+ binding and K^+-Na^+ discrimination. Our results offer insight into a molecular pathway of Na^+ uptake in higher plants. Additional Na^+ uptake pathways may exist and need to be identified. Further structure-function studies of HKT1 should lead to a detailed understanding of the domains involved in K^+-Na^+ discrimination, which in turn may contribute to the future engineering of crop plants with improved salt tolerance.

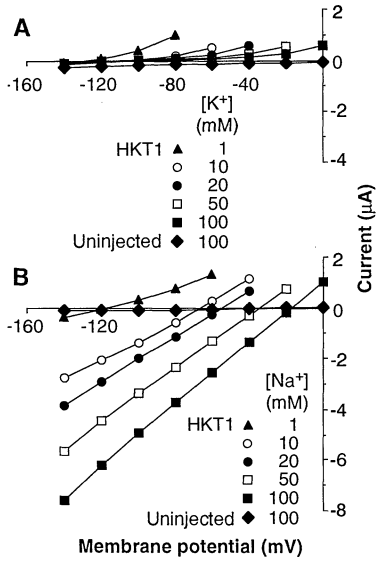

Fig. 4. HKT1 in oocytes mediates low-affinity Na^+ uptake in the absence of K^+, but not K^+ uptake in the absence of Na^+. (**A**) Steady-state current-voltage curves from an HKT1-expressing oocyte exposed to 1, 10, 20, 50, and 100 mM K^+ and from an uninjected oocyte with 100 mM K^+, in the absence of Na^+. (**B**) Analogous experiment with an HKT1-expressing oocyte exposed to 1, 10, 20, 50, and 100 mM Na^+ and with an uninjected oocyte with 100 mM Na^+, in the absence of K^+. Bath solutions were buffered to pH 5.5 (*17*).

REFERENCES AND NOTES

1. H. Greenway and R. Munns, *Annu. Rev. Plant Physiol.* **31**, 149 (1980).
2. T. J. Flowers and A. Läuchli, in *Inorganic Plant Nutrition*, A. Läuchli and R. L. Bieleski, Eds. (Springer-Verlag, Berlin, 1983), vol. 15B, pp. 651–681.
3. M. C. Tarczynski, R. G. Jensen, H. J. Bohnert, *Science* **259**, 508 (1993).
4. T. S. Leyh, *Crit. Rev. Biochem. Mol. Biol.* **28**, 515 (1993); J. R. Murguía, J. M. Bellés, R. Serrano, *Science* **267**, 232 (1995).
5. D. W. Rains and E. Epstein, *Science* **148**, 1611 (1965).
6. ———, *Plant Physiol.* **42**, 314 (1967).
7. R. Serrano, *Plasma Membrane ATPase of Plants and Fungi* (CRC Press, Boca Raton, FL, 1985); T. W. M. Fan, R. M. Higashi, J. Norlyn, E. Epstein, *Proc. Natl. Acad. Sci. U.S.A.* **86**, 9856 (1989); B. J. Barkla and E. Blumwald, *ibid.* **88**, 11177 (1991).
8. S. Schubert and A. Läuchli, *Plant Soil* **123**, 205 (1990).
9. J. I. Schroeder, J. M. Ward, W. Gassmann, *Annu. Rev. Biophys. Biomol. Struct.* **23**, 441 (1994).
10. R. Gaxiola, I. F. de Larrinoa, J. M. Villalba, R. Serrano, *EMBO J.* **11**, 3157 (1992).
11. D. P. Schachtman and J. I. Schroeder, *Nature* **370**, 655 (1994).
12. F. J. M. Maathuis and D. Sanders, *Proc. Natl. Acad. Sci. U.S.A.* **91**, 9272 (1994).
13. The *HKT1* cDNA was subcloned under the control of the yeast *PMA1* gene promoter [R. Serrano, M. C. Kielland-Brandt, G. R. Fink, *Nature* **319**, 689 (1986)] in plasmid pDR195. For uptake experiments, K^+-starved cells [J. Ramos and A. Rodríguez-Navarro, *Eur. J. Biochem.* **154**, 307 (1986)] were analyzed as described (*28*).
14. J. A. Anderson, S. S. Huprikar, L. V. Kochian, W. J. Lucas, R. F. Gaber, *Proc. Natl. Acad. Sci. U.S.A.* **89**, 3736 (1992); J. Ramos, P. Contreras, A. Rodríguez-Navarro, *Arch. Microbiol.* **143**, 88 (1985).
15. G. W. F. H. Borst-Pauwels, *Biochim. Biophys. Acta* **650**, 88 (1981).
16. Exposure in yeast to pH 8 for durations of >8 min resulted in a decrease of Rb^+ uptake compared to pH 6, leading to an apparent proton stimulation (*11*). However, in experiments in which the initial rate of Rb^+ uptake was determined at pH 6 and 8, no differences in initial uptake rates were observed (n = 3). In oocytes, HKT1-mediated outward currents are evident in the absence of external substrate (see Fig. 2) (*11*). The effects of pH on reversal potentials in oocytes (*11*) were obtained by subtraction of HKT1-mediated pre–steady-state outward currents from each other, which gave rise to apparent pH effects (*11*).
17. Oocytes 1 day after injection with 20 ng of *HKT1* mRNA (*11*) were voltage-clamped while bathed in a solution containing 6 mM $MgCl_2$, 1.8 mM $CaCl_2$, and 10 mM Mes-tris (pH 5.5), with osmolality of 240 to 260 mosmol kg^{-1} with D-sorbitol. K^+ and Na^+ were added as glutamate salts.
18. W. Gassmann, F. Rubio, J. I. Schroeder, data not shown.
19. The theoretical reversal potential E_{rev} of a K^+-Na^+ cotransporter is defined by

$$E_{rev} = \frac{58\ mV}{n+m}\left\{m\left[\log\left(\frac{[K^+]_{ext}}{[K^+]_{cyt}}\right)\right] + n\left[\log\left(\frac{[Na^+]_{ext}}{[Na^+]_{cyt}}\right)\right]\right\}$$

where $[K^+]_{ext}$, $[K^+]_{cyt}$, $[Na^+]_{ext}$, and $[Na^+]_{cyt}$ are the external and cytosolic K^+ and Na^+ activities, respectively, and the ratio m:n is the transport stoichiometry. For a stoichiometry of 2 K^+ to 1 Na^+, the shift in reversal potential would be +38.7 mV for an order of magnitude increase in $[K^+]_{ext}$ and +19.3 mV for an order of magnitude increase in $[Na^+]_{ext}$. Assuming physiological values of 0.1 mM for $[Na^+]_{ext}$, 1 mM for $[Na^+]_{cyt}$ (*2*), and 100 mM for $[K^+]_{cyt}$, and a membrane potential of –200 mV (*9*), it can be calculated that a 1 K^+ to 1 Na^+ cotransporter could take up K^+ from soil solutions containing ≥127 nM K^+, and a 2 K^+ to 1 Na^+ cotransporter could take up K^+ from soil solutions containing ≥2.13 μM K^+.
20. A library of 20 × 10^3 randomly mutated HKT1-containing pYES2 plasmids (Invitrogen, San Diego, CA) was generated by treating the plasmid containing *HKT1* cDNA in vitro with 7% hydroxylamine for 2

hours [R. S. Sikorski and J. D. Boeke, in *Guide to Yeast Genetics and Molecular Biology*, C. Guthrie and G. R. Fink, Eds. (Academic Press, San Diego, CA, 1991), vol. 194, pp. 302–318]. Competent cells of K^+ uptake–deficient yeast (*14*) were transformed with the mutagenized HKT1 library. The transformants were eluted and plated in arginine phosphate medium (*28*) containing 0.1 mM K^+ and 500 mM Na^+, which inhibited the growth of the strain expressing wild-type HKT1. Growing colonies were selected, and their plasmids were isolated and reintroduced into yeast to retest for growth in the presence of high [Na^+]. Ten of 60 plasmids conferred the ability to grow at high [Na^+]. The *HKT1* cDNAs of these 10 plasmids were sequenced to identify mutations. The cDNA of the HKT1 mutants was subcloned under the control of the yeast *PMA1* gene promoter, as described (*13*).

21. F. Rubio, W. Gassmann, J. I. Schroeder, data not shown.
22. Abbreviations for the amino acid residues are as follows: A, Ala; F, Phe; L, Leu; and V, Val.
23. For example, at 0.1 mM K^+ and 500 mM Na^+, intracellular K^+ + Na^+ contents were 301 ± 35 nmol mg^{-1} (HKT1), 314 ± 20 nmol mg^{-1} (A240V), and 295 ± 13 nmol mg^{-1} (L247F).
24. W. Gassmann, F. Rubio, J. I. Schroeder, data not shown.
25. Uptake experiments in yeast, in which the background buffer [Na^+] was 11 μM (see Fig. 1), showed that the maximal velocity (V_{max}) for Na^+ uptake at [Na^+] ≥ 1 mM (17 nmol mg^{-1} min^{-1}) was nine times that of the V_{max} for Rb^+ uptake at [Rb^+] ≥ 1 mM (1.8 nmol mg^{-1} min^{-1}).
26. M. R. Sussman, *Annu. Rev. Plant Physiol. Plant Mol. Biol.* **45**, 211 (1994).
27. F. A. Smith and N. A. Walker, *J. Membr. Biol.* **108**, 125 (1989); N. A. Walker and D. Sanders, *Planta (Heidelberg)* **185**, 443 (1991).
28. A. Rodríguez-Navarro and J. Ramos, *J. Bacteriol.* **159**, 940 (1984).
29. We thank R. F. Gaber and A. Rodríguez-Navarro for providing yeast strains, W. B. Frommer for providing the plasmid pDR195 and A. Rodríguez-Navarro, N. M. Crawford, A. Schinder, and J. M. Ward for comments. Supported by U.S. Department of Agriculture (95-37304-2227) and Department of Energy (DE-FG03-34-ER20148) grants and a Presidential Young Investigator Award (to J.I.S.) and a Ministerio de Educación y Ciencia (Spain) postdoctoral fellowship (to F.R.).

14 June 1995; accepted 24 October 1995

A Human Telomeric Protein

Laura Chong, Bas van Steensel, Dominique Broccoli, Hediye Erdjument-Bromage, John Hanish,* Paul Tempst, Titia de Lange†

Telomeres are multifunctional elements that shield chromosome ends from degradation and end-to-end fusions, prevent activation of DNA damage checkpoints, and modulate the maintenance of telomeric DNA by telomerase. A major protein component of human telomeres has been identified and cloned. This factor, TRF, contains one Myb-type DNA-binding repeat and an amino-terminal acidic domain. Immunofluorescent labeling shows that TRF specifically colocalizes with telomeric DNA in human interphase cells and is located at chromosome ends during metaphase. The presence of TRF along the telomeric TTAGGG repeat array demonstrates that human telomeres form a specialized nucleoprotein complex.

Human chromosomes carry a long terminal array of double-stranded TTAGGG hexamers that are maintained by telomerase. Telomeric DNA is thought to form a protective nucleoprotein cap through its association with telomere-specific proteins (*1*). Because the loss of telomere function can induce cell cycle arrest and genome instability, the telomeric complex is likely to be required in all human cells. Changes in the structure and function of human telomeres are thought to play a role in malignant transformation and cellular senescence (*2*, *3*).

Protein components of the telomeric complex have been identified in ciliates and in yeast, but not in vertebrate systems (*1*). Quests for vertebrate telomeric proteins had previously yielded a single candidate factor that could potentially bind along the length of the telomeric TTAGGG repeat array (*4*–*6*). This protein, TRF (telomeric repeat binding factor), associates with double-stranded TTAGGG repeat arrays in vitro and displays strong specificity for vertebrate telomeric DNA (*4*, *5*). TRF does not bind to single-stranded telomeric sequences and does not require the proximity of a DNA terminus for its interaction (*4*). The activity is expressed in nuclei from human, monkey, rodent, and chicken cells, which all carry TTAGGG repeat arrays at their chromosome ends (*4*). Here, we show that TRF is a protein component of human telomeres.

Human TRF (hTRF) activity can be detected in HeLa cell nuclear extracts on

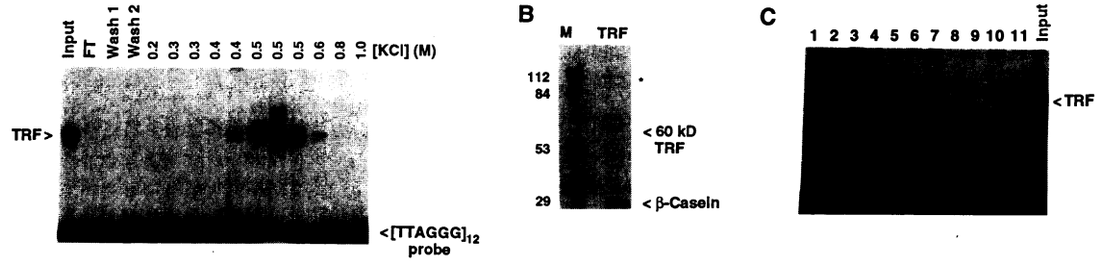

Fig. 1. Purification and identification of the 60-kD hTRF protein. (**A**) Specific DNA affinity chromatography of hTRF. Partially purified HeLa hTRF was applied to a column containing restriction fragments with the sequence $[TTAGGG]_{27}$ coupled to Streptavidin-agarose (*7*). Input, flow-through (FT), and the indicated KCl fractions were assayed for hTRF binding activity with the use of a $[TTAGGG]_{12}$ gel-shift probe. (**B**) Coomassie blue staining pattern of purified hTRF. The 60-kD TRF band is indicated. β-Casein was added to enhance hTRF activity in purified preparations (*7*). The asterisk at the right indicates a ~100-kD protein that is present in some of the hTRF preparations. Marker proteins (M) were prestained. (**C**) Recovery of hTRF activity by elution of the 60-kD protein from SDS-PAGE. Proteins from a gel similar to the one shown in (B) were eluted (*5*, *9*), and hTRF activity was assayed by gel shift with a $[TTAGGG]_{12}$ probe. Lanes 1 to 11 contain proteins isolated from successive gel slices covering the 120- to 20-kD range. Lane 7 contains proteins from the 55- to 65-kD range. (**D**) Analysis of hTRF tryptic peptides by chemical sequencing and laser-desorption mass spectrometry (*10*). Amino acids in lowercase were tentatively assigned; "x" indicates that no identification could be made (*27*). IY indicates calculated initial sequencing yields; *m/z* is the experimental mass of the peptide. [MH^+] denotes the theoretical average isotopic mass of the peptide (plus one proton), calculated from the cDNA-derived sequence (Fig. 3C). M_{ox} refers to methionine sulfoxide (singly oxidized methionine).

D

Peptide	Sequence	IY (pmol)	*m/z*	[MH^+] TRF
T7	EAEEVFEr	1.7	1009.2	1009.06
T8	TLDAqFENdEr	1.4	1337.9	1338.38
T10	TITsQDKPxxNxVxM	1.4	2672.0	2668.80 (M_{ox})
T11	ILLxYK	1.7	–	
T12	IqAIAVxm	0.65	1658.7	1659.80
T13	IFgDPNxxmpf	1.3	1408.5	1406.60 (M_{ox})
T20	xYVNYVLxEK	1.5	1201.4	1202.35
T26	QAxLxEEDK	1.1	–	
T29	TIYICQFTr	1.1	1363.0	1363.53